Appl Nanosci (2016) 6:991–1000
DOI 10.1007/s13204-015-0509-4

ORIGINAL ARTICLE

Effect of preparation conditions on the nanostructure of hydroxyapatite and brushite phases

S. F. Mansour[1] · S. I. El-dek[2] · M. A. Ahmed[3] · S. M. Abd-Elwahab[3] · M. K. Ahmed[3]

Received: 9 September 2015 / Accepted: 30 October 2015 / Published online: 16 November 2015

Abstract Hydroxyapatite (HAP) and dicalcium phosphate dihydrate (brushite) nanoparticles were prepared by co-precipitation method. The obtained products were characterized by X-ray powder diffraction (XRD), Fourier transformation infra-red spectroscopy (FTIR) and thermogravimetric analysis (TGA). Scanning electron microscopy (SEM) and transmission electron microscope (TEM) were used to investigate the morphology of the powdered samples as well as their microstructure, respectively. Brushite samples were obtained in a spherical shape, while hydroxyapatite was formed in a needle and rice shape depending on the pH value.

Keywords Bioceramics · Brushite · Hydroxyapatite

Introduction

In the past few years, calcium phosphate-based materials have been used in many applications in bone regeneration and replacement, teeth pores filling, drug delivery, enhancement of bone growth and in tissue engineering due to their bioactivity and biocompatibility (Navarro et al. 2008; Viswanath and Ravishankar 2008; Rey et al. 2007). Different phases of calcium phosphate nanoparticles (CaP) with different sizes and shapes can be suitable for different purposes (Sørensen and Madsen 2000; Jadalannagari et al. 2011; Oliveira et al. 2007; Ahmed et al. 2008). Several researchers under different preparation conditions studied the synthesis of calcium phosphate extensively (Nilsson et al. 2002; Ren et al. 2012; Kundu et al. 2010a). By varying temperature, pH and initial reagent concentrations, one can obtain different calcium phosphate phases (Kundu et al. 2010b).

It is well known that, hydroxyapatite (HAP: $Ca_{10}(PO_4)_6(OH)_2$) with a hexagonal crystal structure, is one member of the 'apatite' family (Tas 2000; Badraoui et al. 2009). In osteology, calcium is one of the most important inorganic ions, in addition to phosphate given the key component of the mineralized bone matrix. It has a central role in maintaining calcium homeostasis that is very essential for the normal physiological functions (Blair et al. 2007; Peacock 2010). Bone diseases arise when homeostasis is not maintained. Within bone matrix, calcium is important at the whole tissue level, both as a structural component of the mineralized matrix and as a signal transduction molecule for eliciting cellular responses. Owing to its closed structural resemblance to bones and teeth, HAP has attracted much attention as a substitute material for damaged teeth or bones over the last years (Suchanek and Yoshimura 1997; Hench 1991; Ohura et al. 1996).

Calcium hydrogen phosphate dihydrate (DCPD: $CaHPO_4{\cdot}2H_2O$), known as brushite, can be used alone or combined with other materials in the regeneration of bone and various surgical sites in animal models, because it has the ability to be resorbed under physiological conditions (Tamimi et al. 2012; Hench 1998). Therefore, this study is important for bio-mineralization phenomena (Singh et al.

✉ S. I. El-dek
didi5550000@gmail.com

[1] Physics Department, Faculty of Science, Zagazig University, Zagazig, Egypt

[2] Materials Science and Nanotechnology Department, Faculty of Post Graduate Studies for Advanced Science, Beni-Suef University, Beni-Suef, Egypt

[3] Materials Science Lab (1), Physics Department, Faculty of Science, Cairo University, Giza, Egypt

2010). Brushite is also important as soil phosphate fertilizer; it is relatively water soluble as compared with HAP (Pattanayak et al. 2007). It can be used for supplying plant implants with the necessary amount of calcium phosphate (Singh et al. 2010). The physical properties of calcium phosphate ceramics vary strongly according to particle shape, particle size, distribution and agglomeration (Ferreira et al. 2003).

The objective of this work is the preparation of both brushite and hydroxyapatite nanoparticles by simple co-precipitation method to study deeply how the preparation conditions could represent crucial parameters to control calcium phosphate physico-chemical properties. Tuning the properties of such bioceramics could generally improve their use in different biomedical applications owing to their biodegradability, biocompatibility as mentioned above.

Materials and methods

All chemicals were of analytical grade form used without further purification. Disodium hydrogen phosphate (Na_2HPO_4, Merck) and calcium chloride ($CaCl_2{\cdot}2H_2O$, Merck) were used as the starting materials. A diluted solution of ammonium hydroxide (NH_4OH, Merck) and HCl were used as adjusting reagents for pH values.

The flowchart of samples preparation is shown in Fig. 1. Two different groups of samples were prepared using the same procedure, namely co-precipitation method. The first one is concerned with the Ca/P ratio (1:1) and pH values of 4, 5 and 6 adjusted using NH_4OH and/or HCl. The second group in which Ca/P ratio is (5:3) and the pH values were adjusted at 7, 9 and 12 using NH_4OH droplets.

The solutions in both cases were continuously stirred for 24 h (Table 1). The pH value of the suspension was continuously adjusted and maintained at the above-mentioned values during precipitation. The obtained solutions were placed in Teflon flasks and tightly sealed, then aged at room temperature for 24 h to allow precipitation. White precipitated powder was filtered thoroughly and washed several times with double distilled water and finally dried at 50–60 °C for 12 h.

Powder X-ray diffraction analyses were carried out using (analytical-x' pertpro with Cu $k_{\alpha 1}$ target, $\lambda = 1.5404$ Å, 45 kV, 40 mA, The Netherlands) to identify the phase composition and crystallinity of the calcium phosphate compounds. FT-IR spectrometer (Perkin–Elmer system 2000) was used for recording FTIR spectra in the range of 4000–400 cm^{-1}. Thermo-gravimetric analysis (TGA) was carried out from room temperature up to 1200 °C in a DTG-60H SHIMADZU analyzer using an air flow rate of 100 mL/min and a heating rate of 10 °C/min. The surface morphology was studied using scanning electron microscope (SEM) model LEO-1530. The particle size and shape were investigated by transmission electron microscope (TEM) model JEOL/JME—2100.

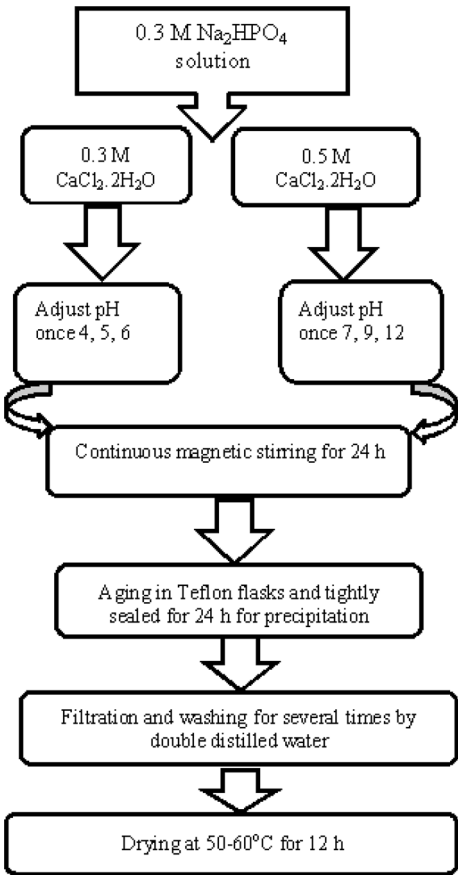

Fig. 1 Flowchart of prepared brushite and hydroxyapatite powder

Table 1 Values of Ca/P, pH values and compound after 24 h reaction time

Compound	Ca/P	pH
DCPD	1:1	5
DCPD	1:1	6
HAP	5:3	7
HAP	5:3	9
HAP	5:3	12

Results and discussion

Structural analysis

X-ray diffraction (XRD)

The sample with low pH value 4 did not precipitate and was completely clear during the experiment. XRD patterns

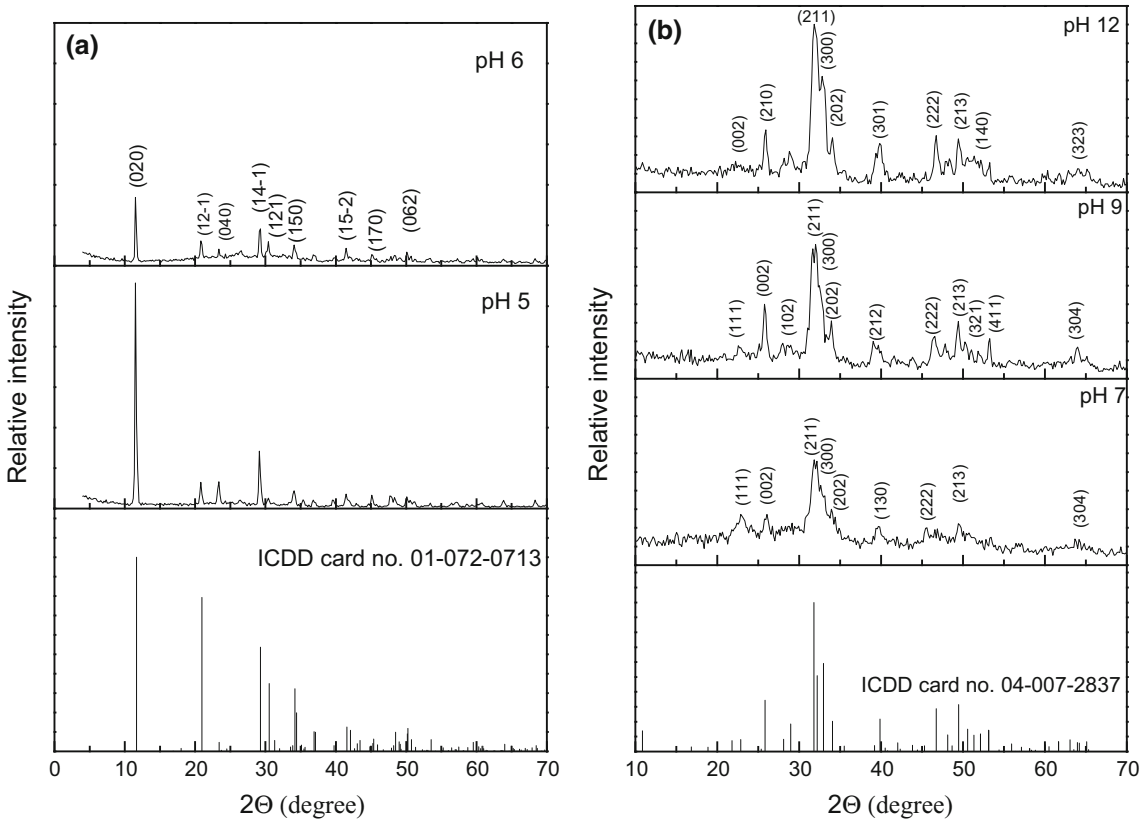

Fig. 2 **a** XRD pattern of calcium phosphate at pH 5, 6, **b** XRD pattern of calcium phosphate at pH 7, 9, 12

Table 2 Variation of crystallite size, particle size, shape, bulk density, theoretical density and relative porosity

Compound	Crystallite size (XRD) (nm)	Particle size (TEM)		Shape	Density (g/cm^3)	Theoretical density (g/cm^3)	Porosity %
		Dia.(nm)	Length (nm)				
DCPD pH 5	55	50–90[a]	–	Sphere	2.13	2.32	8.24
DCPD pH 6	41	5–10	50–150	Fiber network	1.75	2.32	24.71
HAP pH 7	5	5–10	150–200	Needle	1.54	3.23	53.58
HAP pH 9	15	20–30	200–300	Rods	1.94	3.16	38.74
HAP pH 12	16	10–20	40–60	Rice	1.93	3.17	39.21

[a] Spherical shape

for the samples of the first group synthesized at pH 5 and 6 represent brushite with single phase as shown in Fig. 2a and agree well with the ICDD card no. 01-072-0713. These patterns show that the peaks of brushite at pH 5 have higher intensities than those at pH 6. The crystallinity of these samples was found to decrease with increasing pH value as reported in Table 2.

Figure 2b illustrates XRD patterns for the samples of the second group prepared at pH values 7, 9 and 12, which demonstrate that the pH value takes the upper hand in the formation of HAP. Phase analysis was identified using ICDD card no. 04-007-2837 for HAP. It is clearly noted that the sample with higher pH has sharper diffraction peaks (larger crystallite size) than other samples. These results indicate that HAP at pH 12 has larger crystallite size as shown in Fig. 2b. The broad pattern of the samples was attributed to the formation of poor crystalline HAP, which leads to higher dissolution compared with well-crystallized HAP. Moreover, it was reported that the crystallinity is a crucial factor that affects the biological behavior (Uehiraa et al. 2013; Dorozhkin 2010; Fulmer et al. 2002). Hong et al. have demonstrated that osteoblasts exhibited a high cellular activity such as adhesion on the low-crystallinity HAP thin film (Hong et al. 2003). The gradual increase in

the intensity of HAP peaks with increasing the pH value indicates further nucleation growth of the hexagonal nanocrystals.

Crystallite size was calculated for HAP powder using Scherrer's formula and reported in Table 2. The crystallite size of the HAP crystals was 5, 15, 16 nm for pH values of 7, 9 and 12, respectively, while in the case of brushite phase, the crystal size was 55 and 41 nm at pH 5, 6, respectively. The lattice parameters for HAP were $a = 9.399$ Å and $c = 6.890$ Å at pH = 7. The unit cell volume was 527.19 (Å)^3, 527.44 (Å)^3 and 526.249 (Å)^3 for the pH values 7, 9 and 12, respectively, which agree well with that reported with ICDD card no. 04-007-2837. The theoretical density D_x was determined using the formula:

$$D_x = \frac{ZM}{NV} \quad (1)$$

where M is the molecular weight of the sample, N is Avogadro's number, Z is the number of molecules per unit cell and V is the unit cell volume calculated from XRD data (Ahmed et al. 2003; Cullity 1978).

The results in Table 2 show that the above investigated samples possess a considerable amount of apparent porosity (39–53 %) as calculated from

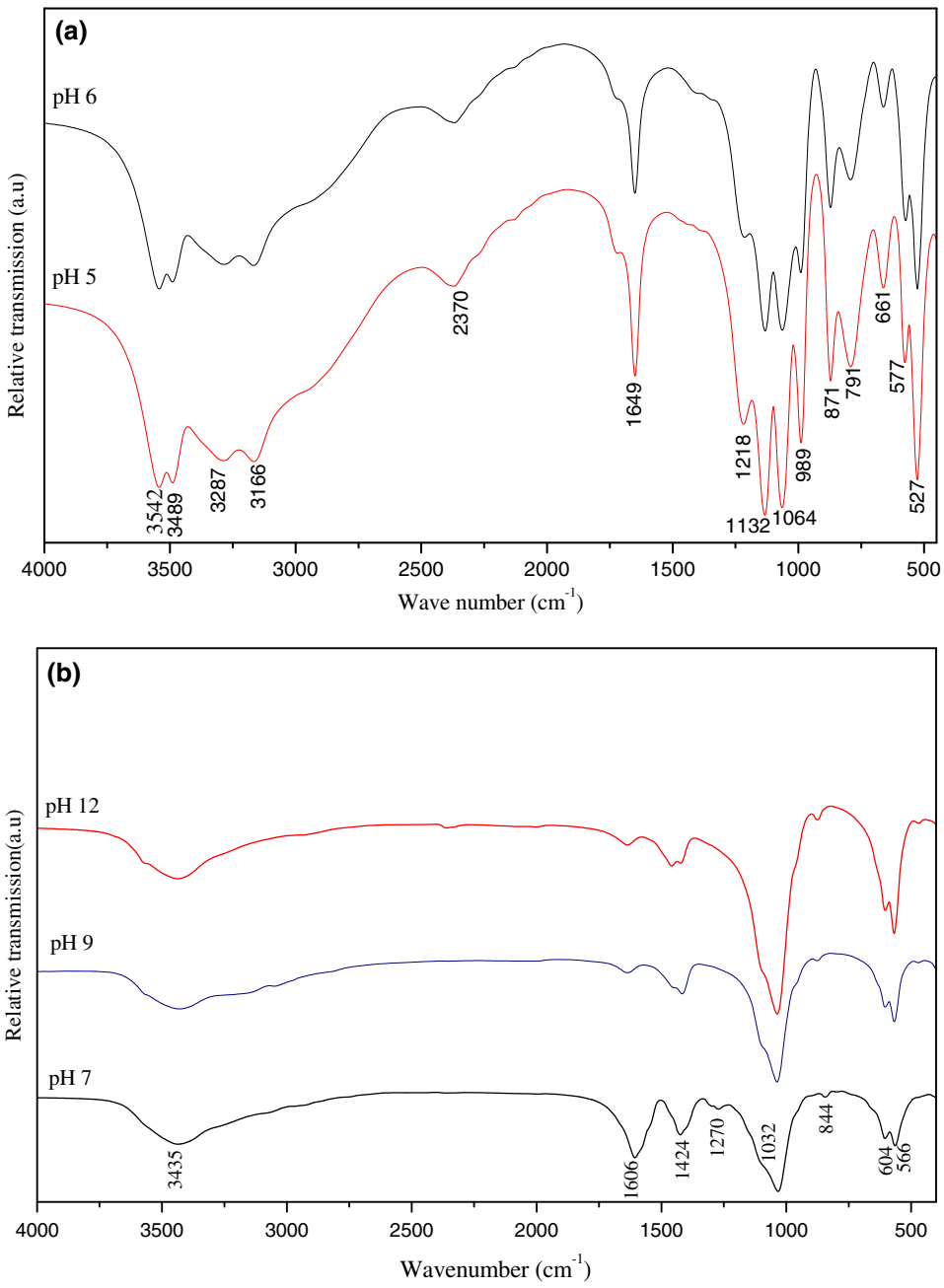

Fig. 3 FTIR spectra of calcium phosphate: **a** pH 5, 6, **b** pH 7, 9, 12

Table 3 Characteristic transmittance infrared bands of brushite and hydroxyapatite at different pH values

pH 5	pH 6	Assignment (Singh et al. 2010; Mandel and Tas 2010; Maity et al. 2011)	pH 7	pH 9	pH 12	Assignment (Ahmed et al. 2014; Markovic et al. 2011; Alobeedallah et al. 2011; Morales et al. 2013; Minh et al. 2013; Asep and Sopyan 2009)
527	526	v_4 of P–O–P bending	470	471	474	Vibration O–P–O
577	573	v_4 of P–O–P bending	566	567	567	Vibration O–P–O
661	661	Water liberation	604	603	606	Vibration O–P–O mode
791	791	Water liberation	844	872	873	v_2 bending of CO_3^{2-} ions
871	872	Stretching mode of (HPO_4^{2-})	1032	1034	1036	v_3 vibration of PO_4^{3-} ions
			1270	–	–	Confirm CO_3^{2-}
989	990	v_1 stretching vibration of PO_4^{3-}	1424	1420	1421	v_3 stretching of CO_3^{2-} ions
1064	1063	v_3 (P–O) Stretching of the PO_4^{3-} group	–	1458	1460	
1132	1131	v'_6 and v''_6 of HPO_4^{2-} group				
1218	1215	Bending (O–H) in HPO_4^{2-} group	1606	1640	1632	Absorbed water
1649	1651	Bending mode of H_2O	–	2359	2360	Absorbed water
2370	2370	Overtone or combination band				
3166	3164	(O–H) stretching of water	3435	3435	3433	O–H stretching
3287	3285					
3489	3486	Stretching of water [v_s (O–H)]				
3542	3542					

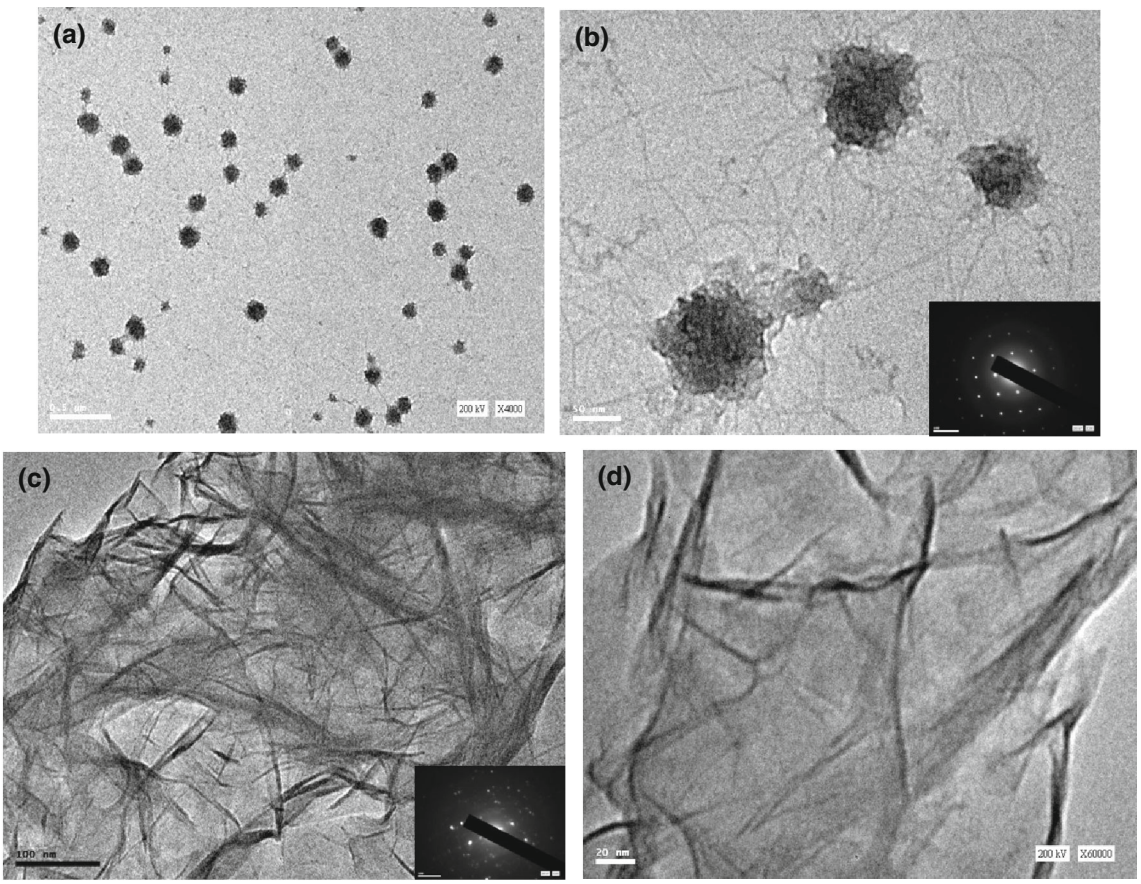

Fig. 4 TEM micrographs of brushite phase: **a**, **b** pH 5, **c**, **d** pH 6

$$P = \left(1 - \frac{D}{D_x}\right) \times 100\,\% \quad (2)$$

where P is the porosity, and D and D_x are the experimental and theoretical densities, respectively (Ahmed et al. 2003).

FTIR analysis

The structure of the samples prepared at pH values of 5 and 6 was investigated by FTIR spectra, as shown in Fig. 3a and presented in Table 3. From the figure, there is a neglected shift between pH 5 and 6. The absorption bands at 661–527 and 1218–989 cm^{-1} are due to v_4 bending vibration of P–O–P mode. The vibrations at 871 and 791 cm^{-1} are attributed to the P–O–H vibrations for inorganic Ca–P component (Mandel and Tas 2010). The four bands, 871, 989, 1064 cm^{-1} and 1132 cm^{-1} are originating to the (HPO_4^{2-}) stretching in both dicalcium phosphates, i.e.; monotite (DCPA) and brushite. A band at 989 cm^{-1} is assigned from the P–O(H) symmetric stretching vibration of PO_4^{3-} group (Singh et al. 2010; Maity et al. 2011). Moreover, band near to 1064 cm^{-1} is reffered to the v_3 stretching mode of the PO_4^{3-} group. A band around 1132 cm^{-1} was attributed to the v'_6 and v''_6 of HPO_4^{2-} ions in brushite (Maity et al. 2011).

Further investigation of the FTIR spectra revealed that the band at 1649 cm^{-1} was ascribed to the bending mode of H_2O. The bands at 3166, 3287, 3489 and 3542 cm^{-1} corresponded to stretching vibration of water [v_s (O–H)] (Singh et al. 2010; Ahmed et al. 2014). The bands between 3000 and 3600 cm^{-1} show the presence of DCPD but not in its anhydrous form DCPA (Singh et al. 2010; Zou et al. 2012).

In the spectrum shown in Fig. 3b for the samples prepared at pH (7, 9, 12), the absorption bands at 3435 and 1606 cm^{-1} were assigned to the absorbed water (Markovic et al. 2011). The bands at 1424 and 844 cm^{-1} were attributed to the vibrations of CO_3^{2-} groups absorbed from the ambient atmosphere (Alobeedallah et al. 2011). The presence of carbonate results from the ambient CO_2 dissolved during the crystallization process, whereas HAP crystals are very susceptible to CO_2. It is observable that all

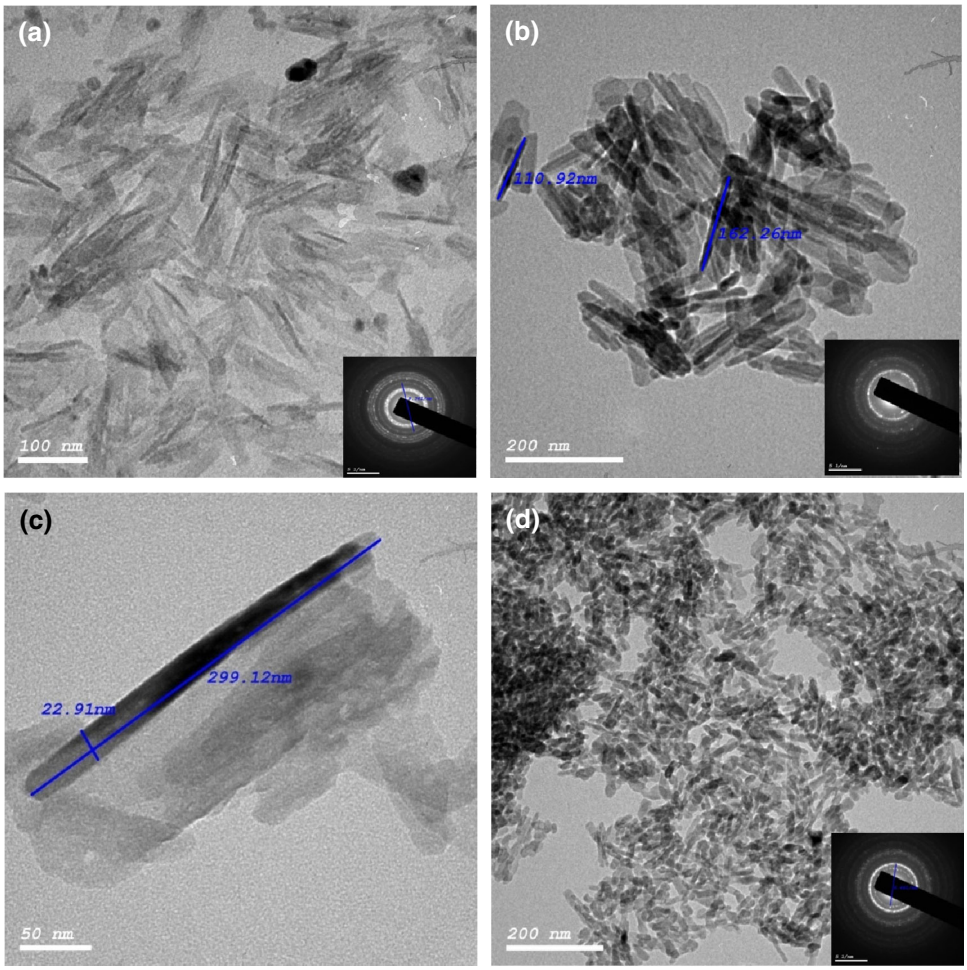

Fig. 5 TEM micrographs of hydroxyapatite phase: **a** pH 7, **b**, **c** pH 9, **d** pH 12

samples are classified as B-type (where CO_3^{2-} substitutes phosphate position) (Ahmed et al. 2014). It should be mentioned that carbonate substitution has a critical role in the crystal structure, stability and biological activity (Morales et al. 2013; Minh et al. 2013).

The appearance of a band at 1270 cm^{-1}, where CO_3^{2-} possibly replaces PO_4^{3-}, confirms the identity of carbonate (Asep and Sopyan 2009). The characteristic bands of PO_4^{3-} appeared at 566, 604 and 1032 cm^{-1} where the bands at 566 and 604 cm^{-1} were assigned to the vibration of the O–P–O mode (Markovic et al. 2011). It is observed that the intensities of the bands were increased by increasing the pH value, as a result of the improvement of the crystallinity of the investigated samples. These results are also in good agreement with those mentioned in XRD results Fig. 2b. There is little shift with different pH values, and the assigned bands are reported in Table 3.

Microstructural and morphological features

TEM

Figure 4a, b shows the transmission electron micrograph of the brushite nanoparticles at pH 5. The particles are formed in spherical shapes, with sizes ranging from 50 to 90 nm. With further increase in the magnification, each particle looks like a silk ball with yarns linking between them. These silk filaments have different lengths with a diameter around 2–6 nm. TEM micrograph of brushite at pH 6 shown in Fig. 4c, d reveals that the particles are formed in a fiber network with lengths from 100 to 150 nm. The corresponding selected area electron diffraction SAED pattern shows that the particles are polycrystalline and have a preferred orientation. This special morphology of these samples facilitates their easy attachment to biological cells.

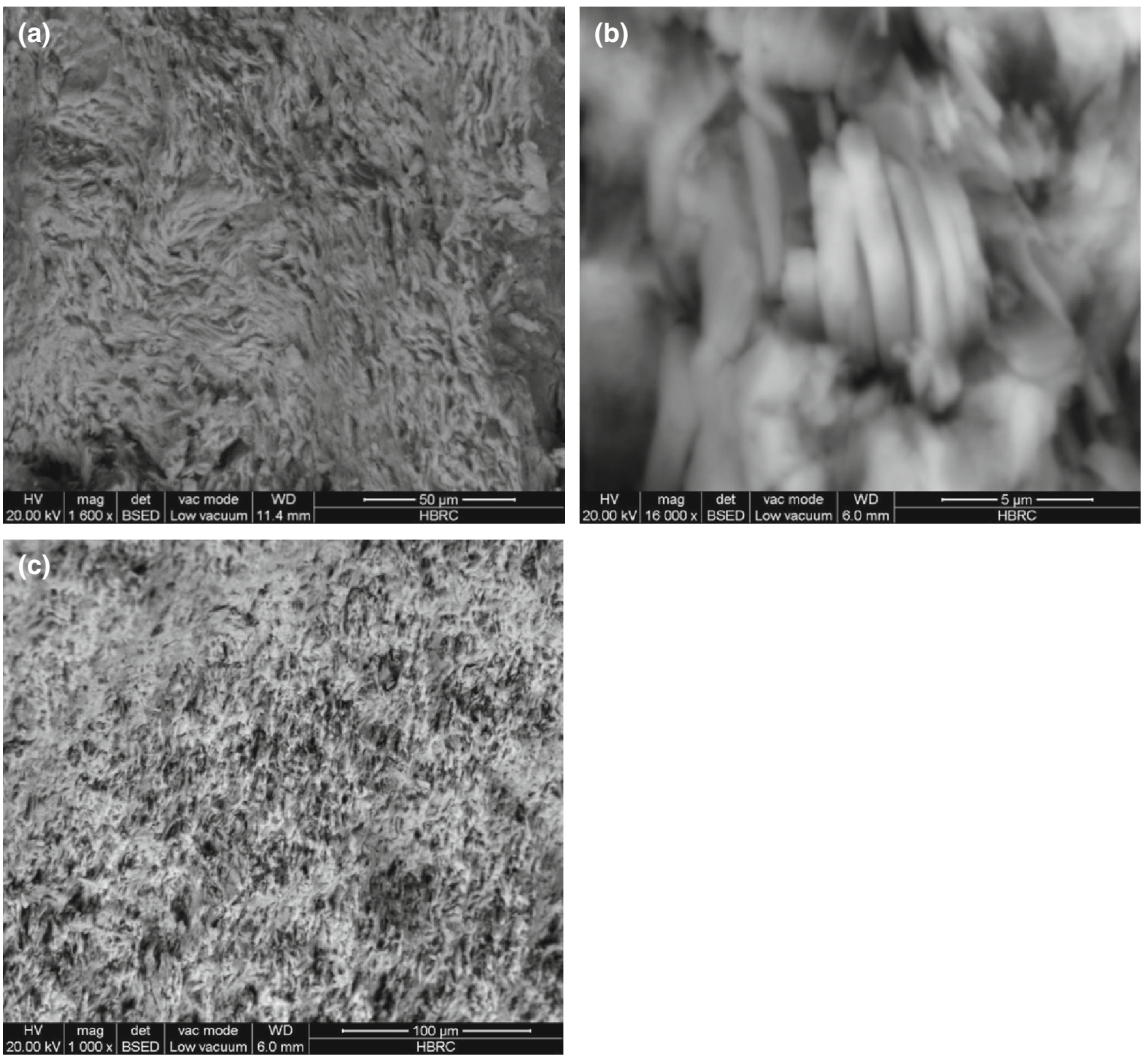

Fig. 6 SEM micrograph of brushite phase: **a** pH 5, **b**, **c** pH 6

Figure 5a shows the TEM micrograph of nano-HAP at pH 7. The HAP nanoparticles were uniform in both morphology and size. The sample appears as needle shape crystals, with a diameter around 5–10 nm with length 150–200 nm. SAED is shown in the inset of Fig. 4a and reveals diffraction rings indicating twin crystal structure and demonstrates that the needles are polycrystalline rings with a preferred direction (100) as indicated by XRD.

TEM of HAP at pH 9 together with the SAED was demonstrated in Fig. 5b, c. The micrograph shows nanorods with diameters ranging from 20 to 30 nm with a wide range of lengths starting from 200 to 300 nm. The rod shape becomes clear and uniform by increasing the magnification with a constant aspect ratio Fig. 5c.

HAP with these dimensions (~20 nm) resembles to the basic building blocks of enamel rods. In addition, it has been observed that HAP nanoparticles can be self-combined to form enamel-like structures in vitro and it could be adsorbed onto the enamel surface strongly. Therefore, it could be used to improve the repair of the enamel surface (Chen et al. 2005; Liu et al. 1998).

Figure 5d illustrates the TEM micrographs of HAP at pH 12 together with SAED, which appeared as rice shape with diameters in the range of 10–20 nm in length does not exceed 60 nm. It is clear that the particle size becomes shorter, which is attributed to the isotropic crystal growth at higher pH values. On the contrary, the nanoparticles synthesized at low pH have more complicated shapes (Liu et al. 1998).

SEM

Figure 6a illustrates the morphology of the nanobrushite sample at pH 5 which appears as homogenous surface with irregular particles, a small amount of apparent porosity. This irregularity appears on the surface as roughness,

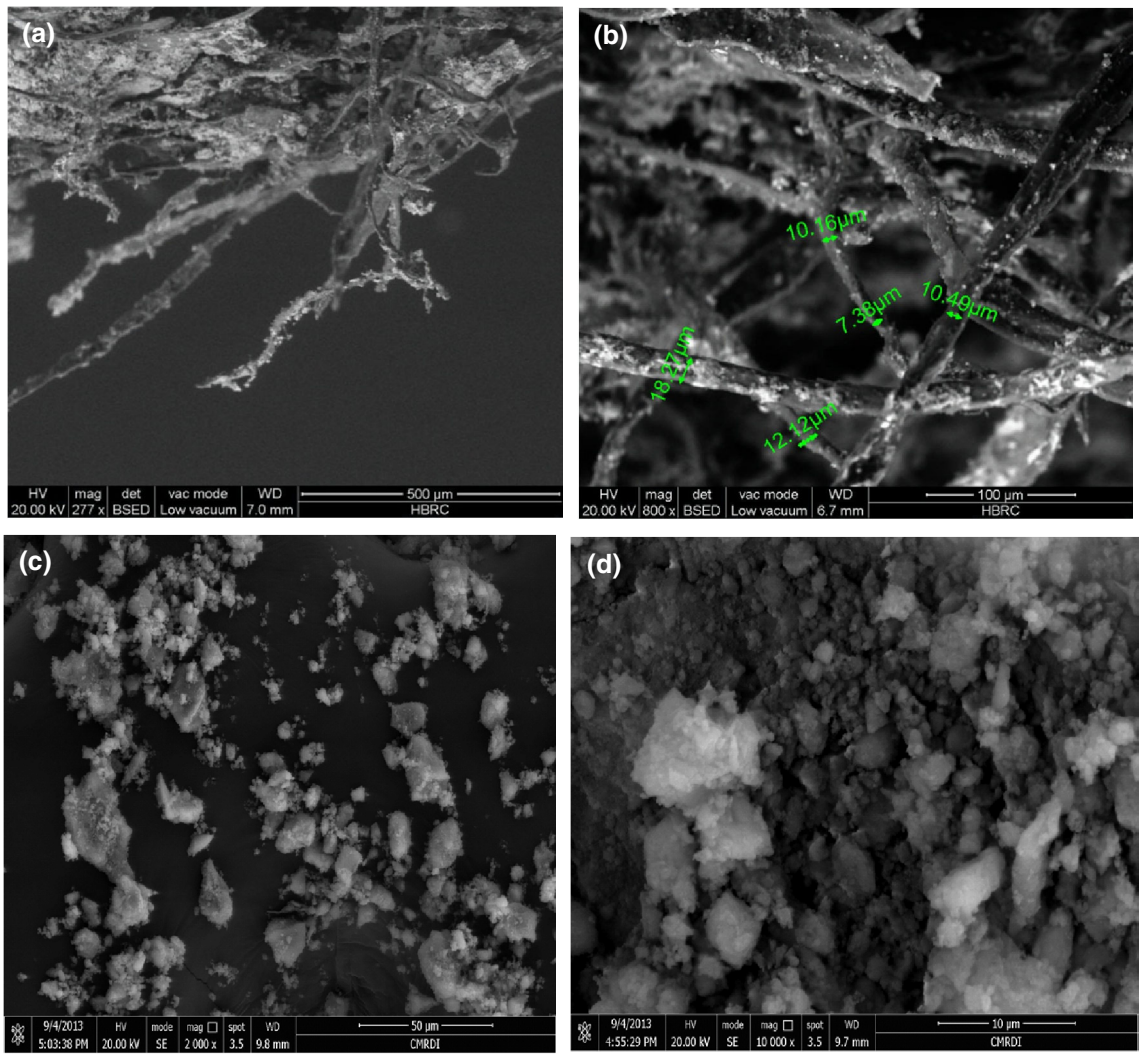

Fig. 7 SEM micrograph of hydroxyapatite phase: **a**, **b** pH 7, **c**, **d** pH 12

which could improve the osseointegration as well as the biocompatibility leading to the positive effect on inflammatory reactions (Morales et al. 2013; Müller 2010).

For the sample prepared at pH 6; Fig. 6b, c, the particles appeared as a bundle of fibers arranged in a certain direction with irregular pores (24.71 %) as shown in Table 2. The morphological feature of the samples with pH 7 and 12 was demonstrated by SEM as shown in Fig. 7a–d. The nanoparticles appeared as micro fibers with diameters in ranges of 5–10 μm and length exceeding 900 μm at pH 7 as in Fig. 7a, b. Figure 7c, d reveals agglomerated grains with various sizes from 0.5 to 10 μm of pH 12.

Thermal analysis

TGA

Thermo-gravimetric analysis was carried out with the temperature range 30 to 1200 °C in the air at a heating rate 10 °C/min. Figure 8 shows the TGA of brushite at pH 5 and HAP at pH 9 and 12. For all the samples, the analysis of weight loss is observed in three stages. The first one was related to the water removal from the precipitated powders; the second and third loss ones resulted from the decomposition of organic components in the raw materials (Fulmer et al. 2002). The third stage illustrates the thermal stability of the samples from 550 to 1200 °C. Total weight loss of the brushite at pH 5, HAP at pH 9 and 12 was 21.15, 6.91 and 6.283 %, respectively, at the end of the experiment at 1200 °C. This emphasizes the hypotheses that the higher pH values lead to higher thermal stability which is in good agreement with the reported work (Ahmed et al. 2014). The advantage of thermal analysis is to specify the working temperature range at which the bioceramics are applicable. Another benefit is to determine the exact temperature of phase transformation.

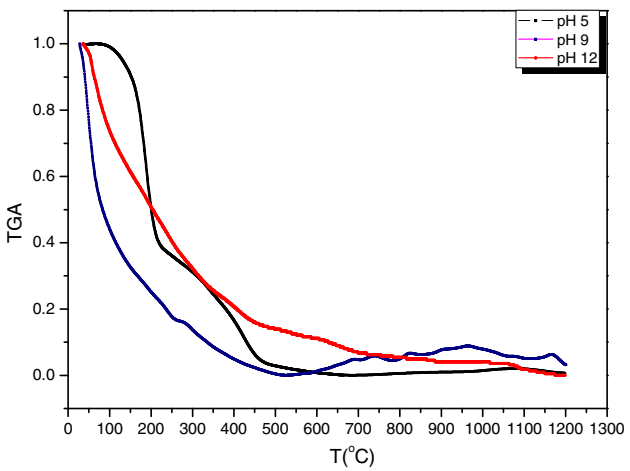

Fig. 8 TGA of brushite phase at pH 5, HAP at pH 9 and 12

Conclusion

Brushite and HAP nanoparticles were successfully obtained from the homogeneous precipitation as perfect mono dispersed particles with sizes ranging from 50 to 200 nm. The nano-HAP particles will be extensively investigated for future use in biomedical applications such as bioactive ceramics for bone substituting materials and tissue scaffold. When regulating the preparation conditions, mainly pH and Ca/P ratio, different micro structures could be tailored to achieve fiber network, silk ball, short and long nanorods.

Compliance with ethical standards

Conflict of interest No conflict of interest exists.

References

Ahmed MA, Ateia E, El-Dek SI (2003) Rare earth doping effect on the structural and electrical properties of Mg–Ti ferrite. Mater Lett 57:4256–4266

Ahmed MA, Okasha N, El-Dek SI (2008) Preparation and characterization of nanometric Mn ferrite via different methods. Nanotechnology 19:065603

Ahmed MA, Mansour SF, El-dek SI, Abd-Elwahab SM, Ahmed MK (2014) Characterization and annealing performance of calcium phosphate nanoparticles synthesized by co-precipitation method. Ceram Int 40:12807–12820

Alobeedallah H, Ellis LJ, Rohanizadeh R, Hans C, Dehghani F (2011) The preparation of nanostructured hydroxyapatite in organic solvents for clinical applications. Trends Biomater Artif Organs 25:12–19

Asep F, Sopyan L (2009) Low temperature hydrothermal synthesis of calcium phosphate ceramics: effect of excess Ca precursor on phase behaviour. Indian J Chem 48:1492–1500

Badraoui B, Aissa A, Bigi A, Debbabi M, Gazzano M (2009) Synthesis and characterization of $Sr_{(10-x)}Cd_x(PO_4)_6Y_2$ ($Y = OH^-$ and F^-): a comparison of apatites containing two divalent cations. Mater Res Bull 44:522–530

Blair HC, Schlesinger PH, Huang CLH, Zaidi M (2007) Calcium signalling and calcium transport in bone disease. Subcell Biochem 1:539–562

Chen H, Clarkson BH, Sun K, Mansfield JF (2005) Self-assembly of synthetic hydroxyapatite nanorods into an enamel prism-like structure. J Colloid Interface Sci 288:97–103

Cullity BD (1978) Elements of X-ray diffraction, 2nd edn. Addison-Wesley Publishing Company Inc., London

Dorozhkin SV (2010) Bioceramics of calcium orthophosphates. Biomaterials 31:1465–1485

Ferreira A, Oliveira C, Rocha F (2003) The different phases in the precipitation of dicalcium phosphate dihydrate. J Cryst Growth 252:599–611

Fulmer MT, Ison IC, Hankermayer CR, Constantz BR, Ross J (2002) Measurements of the solubilities and dissolution rates of several hydroxyapatites. Biomaterials 23:751–755

Hench LL (1991) Bioceramics: from concept to clinic. J Am Ceram Soc 74:1487–1510

Hench LL (1998) Bioceramics. J Am Ceram Soc 81:1705–1728

Hong J, Kim YJ, Lee H, Lee W, Ko JS, Kim H (2003) Osteoblastic cell response to thin film of poorly crystalline calcium phosphate apatite formed at low temperatures. Biomaterials 24:2977–2984

Jadalannagari S, More S, Kowshik M, Ramanan SR (2011) Low temperature synthesis of hydroxyapatite nano-rods by a modified sol–gel technique. Mater Sci Eng C 31:1534–1538

Kundu B, Soundrapandian C, Nandi SK, Mukherjee P, Dandapat N, Roy S, Datta BK, Mandal TK, Basu D, Bhattacharya RN (2010a) Development of new localized drug delivery system based on ceftriaxone-sulbactam composite drug impregnated porous hydroxyapatite: a systematic approach for in vitro and in vivo animal trial. Pharm Res 27:1659–1676

Kundu B, Lemos A, Soundrapandian C, Sen PS, Datta S, Ferreira JM, Basu D (2010b) Development of porous HAp and β-TCP scaffolds by starch consolidation with foaming method and drug-chitosan bilayered scaffold based drug delivery system. J Mater Sci Mater Med 21:2955–2969

Liu Q, de Wijn JR, de Groot K, Blitterswijk CAV (1998) Surface modification of nano-apatite by grafting organic polymer. Biomaterials 19:1067–1072

Maity JP, Lin TJ, Cheng HH, Chen C, Reddy AS, Atla SB, Chang Y, Chen H, Chen C (2011) Synthesis of brushite particles in reverse micro emulsions of the biosurfactant surfactin. Int J Mol Sci 12:3821–3830

Mandel S, Tas AC (2010) Brushite (CaHPO4·2H2O) to octacalcium phosphate (Ca8(HPO4)2(PO4)4·5H2O) transformation in DMEM solutions at 36.5 °C. Mater Sci Eng C 30:245–254

Markovic S, Veselinovic L, Lukic MJ, Karanovic L, Bracko I, Ignjatovic N, Uskokovic D (2011) Synthetical bone-like and biological hydroxyapatites: a comparative study of crystal structure and morphology. Biomed Mater 6:045005

Minh DP, Tran ND, Nzihou A, Sharrock P (2013) Carbonate-containing apatite (CAP) synthesis under moderate conditions starting from calcium carbonate and orthophosphoric acid. Mater Sci Eng C 33:2971–2980

Morales JG, Iafisco M, López JMD, Sarda S, Drouet C (2013) Progress on the preparation of nanocrystalline apatites and surface characterization: overview of fundamental and applied aspects. Prog Cryst Growth Charact Mater 59:1–46

Müller B (2010) Tailoring biocompatibility: benefitting patients. Mater Today 13:58

Navarro M, Michiardi A, Castano O, Planell J (2008) Biomaterials in orthopaedics. J R Soc Interface 5:1137–1158

Nilsson M, Fernandez E, Sarda S, Lidgren L, Planell JA (2002) Characterization of novel calcium phosphate/sulphate bone cement. J Biomed Mater Res 61:600–607

Ohura K, Bohner M, Hardouin P, Lemaitre J, Pasquier G, Flautre B (1996) Resorption of, and bone formation from, new β-tricalcium phosphate-monocalcium phosphate cements: an in vivo study. J Biomed Mater Res 30:193–200

Oliveira C, Georgieva P, Rocha F, Ferreira A, Azevedo SF (2007) Dynamical model of brushite precipitation. J Cryst Growth 305:201–210

Pattanayak DK, Dash R, Prasad RC, Rao BT, Mohan TRR (2007) Synthesis and sintered properties evaluation of calcium phosphate ceramics. Mater Sci Eng, C 27:684–690

Peacock M (2010) Calcium metabolism in health and disease. J Am Soc 5:23–30

Ren F, Ding Y, Ge X, Lu X, Wang K, Leng Y (2012) Growth of one-dimensional single-crystalline hydroxyapatite nanorods. J Cryst Growth 349:75–82

Rey C, Combes C, Drouet C, Sfihi H, Barroug A (2007) Physico-chemical properties of nanocrystalline apatites: Implications for biominerals and biomaterials. Mater Sci Eng C 27:198–205

Singh S, Singh V, Aggarwal S, Mandal UK (2010) Synthesis of brushite nanoparticles at different temperatures. Chem Pap 64:491–498

Sørensen JS, Madsen HEL (2000) The influence of magnetism on precipitation of calcium phosphate. J Cryst Growth 216:399–406

Suchanek W, Yoshimura M (1997) Hydroxyapatite ceramics with selected sintering additives. Biomaterials 13:923–933

Tamimi F, Sheikh Z, Barralet J (2012) Dicalcium phosphate cements: brushite and monetite. Acta Biomater 8:474–487

Tas AC (2000) Synthesis of biomimetic Ca-hydroxyapatite powders at 37 °C in synthetic body fluids. Biomaterials 21:1429–1438

Uehiraa M, Okadab M, Takedab S, Matsumoto N (2013) Preparation and characterization of low-crystallized hydroxyapatite nano porous plates and granules. Appl Surf Sci 287:195–202

Viswanath B, Ravishankar N (2008) Controlled synthesis of plate-shaped hydroxyapatite and implications for the morphology of the apatite phase in bone. Biomaterials 29:4855–4863

Zou Z, Lin K, Chen L, Chang J (2012) Ultrafast synthesis and characterization of carbonated hydroxyapatite nanopowders via sonochemistry-assisted microwave process. Ultrason Sonochem 19:1174–1179